Wide Range Multi-level DC-DC Converter with TCM for High Voltage Applications

Takashi Ohno[1], Rintaro Kusui[1], Hiroki Watanabe[1], Jun-ichi Itoh[1], and Takuya Kataoka[2]
[1] Nagaoka University of Technology, Japan
[2] Mitsubishi Electric Corp., Japan

***Abstract*— This paper proposes a control method based on Triangular Current Mode (TCM) for a Current-Fed Dual Active Bridge (DAB) converter, which uses a three-level flying capacitor converter in order to accept high voltage(1500V) output. The proposed control method achieves the high-efficiency region in a wide operation range. Additionally, the proposed control performs the Zero Voltage Switching in a wide operation range. Also, the TCM is controlled at a variable frequency to keep the negative current constant. As a result, the operation range is limited because the switching frequency of the power converter is often applied to several kilo-Hz in high-power applications. In order to solve this problem, this paper also proposes that the full-bridge and half-bridge operation is adopted using the multi-level flying capacitor configuration. In the experimental results, the operation range of the proposed control is extended by 70% compared to that of the conventional Current-Fed DAB converter.**

***Index Terms*—Current-Fed Dual Active Bridge converter, Multi-level, Triangular Current Mode, Zero Voltage Switching**

I. INTRODUCTION

Recently, medium voltage DC distribution systems have been widely developed owing to their high system efficiency and compatibility with renewable energy sources such as Photovoltaic (PV) and fuel cells [1]-[3]. In these systems, an isolated DC-DC converter is required to interface the converter between the DC-bus and energy sources or batteries.

Several isolated DC-DC converters have been widely developed for their applications [4]-[8]. A Dual Active Bridge (DAB) converter is one of the strong candidates because of its attractive advantages, e.g., 1) simple configuration, 2) galvanic isolation capability, and 3) Zero Voltage Switching (ZVS) operation for low switching losses. However, the DAB converter has narrow high-efficiency characteristics when the voltage transfer ratio does not match the turn ratio of the high-frequency transformer. Additionally, the large ripple current may increase the volume of the filter capacitor.

In contrast, the modulation and modified circuit configuration of the DAB converter are proposed to improve the performance. In particular, the modulation method to expand the ZVS range [9]-[11] and to achieve the minimum transformer current RMS [12]-[14] have been proposed. Specifically, extended-phase shift (EPS) control, dual-phase shift control, and triple-phase shift (TPS) control have been proposed as a modulation method that achieves ZVS over a wide range and a minimum current RMS. Additionally, the operating frequency of the converter can also be utilized. With the increase of control degree of freedom, the challenge for these methods is difficult to determine the optimal combinations of multiple control variables, which could include phase shift ratio, two duty cycles and the operating frequency. As the approach from the circuit topology, a T-type DAB with the switching operation mode [15], a six-arm converter with series-parallel switching [16], and the Neutral Point Clump (NPC) based three-level DAB converter [17] have been proposed. The T-type topology has improved light load efficiency during voltage fluctuations. However, T-type is not enough to achieve high withstand voltage. A six-arm converter has achieved ZVS over a wide voltage range. However, efficiency at medium to light loads is very poor. The NPC-based three-level converter can be achieved high efficiency operation over a wide voltage range and high withstand voltage. In contrast, the challenge for NPC converter is many additional components. Additionally, these converters increase the volume of the filter capacitor because of the large ripple current.

By contrast, a Current-Fed DAB converter has been studied in order to reduce input current ripple or improve efficiency for several applications [18]-[19]. The Current-Fed DAB converter reduces the ripple current by the inductor, which is connected to the DC input side. In particular, the DC capacitor voltage control matches the turn ratio of the high-frequency transformer. In addition, the Triangular Current Mode (TCM) operation for the Current-Fed DAB converter has been proposed [20]. As a result, the Current-Fed DAB converter achieves ZVS in wide input voltage conditions. However, the switching frequency drastically increases at light load conditions because the TCM operation is implemented based on a variable switching frequency operation. Generally, the high-power DC-DC converters for more than several hundred kilo-watts commonly accept IGBT modules because the IGBT module has a high voltage and power rating and is relatively inexpensive. Moreover, the switching speed of the IGBT module is slower than the SiC module. As a result, the operating area for the TCM is limited by the switching frequency.

This paper proposes the TCM operation for a Current-Fed DAB converter, which has a three-level Flying Capacitor (FC) converter on the secondary side, in order to obtain high converter efficiency in light load. The original points of this paper are two things; the first, the flying capacitor-based three-level converter is used in the secondary side and combined by the TCM; the second, the

transformer voltage is changed by switchover the FB and HB modes depending on the input voltage and the transmission power. Therefore, the lower voltage rating devices are used for each switching device. In addition, the FB and HB modes of a three-level converter adjust the transformer voltage in order to reduce the switching frequency of the Current-Fed DAB converter. This paper is organized as follows; first, the circuit configuration is introduced. Second, the TCM operating area expansion method and the operation principle of each operation mode are explained. Third, the efficiency analysis of conventional and proposed methods is compared. Finally, a prototype of 1500 V output voltage and 12.8-kW output power is demonstrated by the experiment at several power conditions in order to confirm the validity of the proposed control of FB mode and HB mode with TCM.

II. Circuit Configuration

Fig. 1 shows the proposed Current-Fed DAB converter with a three-level flying capacitor converter. The primary side converter consists of an H-bridge converter which integrates the interleaved DC-DC converter. This converter has the voltage control capability for the DC capacitor voltage V_C to match the voltage ratio with the turn ratio of the transformer. The current mode of i_{LCA}, and i_{LCB} applies the TCM operation to achieve ZVS for the primary side H-bridge converter. The TCM operation increases the current ripple compared to the Continuous Current Mode (CCM) to generate a small negative current. The interleaved converter reduces the ripple current of the DC power sources by phase-shifted modulation. A three-level flying capacitor converter is applied to accept the high-voltage secondary DC side. The voltage rating of each switching device is reduced to half of the output voltage V_{out}.

III. Proposed TCM operating area expansion method

A. Triangular Current Mode Operation

Fig.2 shows the switching pattern of the primary side H-bridge converter. The switching duty ratio of the typical DAB converter is set to 0.5. Compared to that, the Current-Fed DAB converter applies the primary DC capacitor voltage control to adjust the voltage ratio between the input and output. That is, the switching duty ratio is carried out depending on the boost ratio of the DC capacitor voltage. In addition, the variable switching frequency control is implemented to achieve the TCM operation. As a result, the switching frequency increases at light load conditions to adjust the negative inductor current. However, the switching frequency in the TCM is limited by the performance of the switching devices. As a result, the TCM operation cannot realize in the light load condition.

This paper proposed to use two operation modes, Full-Bridge (FB) and Half-Bridge (HB) modes on the secondary side, in order to expand the operating area of the TCM operation.

The relationship between input power and the switching frequency is expressed as

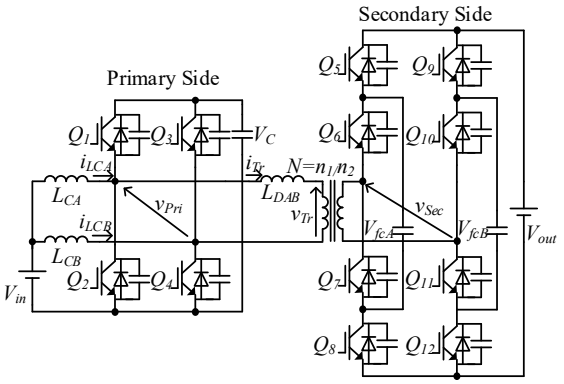

Fig. 1. Circuit configuration of Current-Fed DAB with a three-level flying capacitor converter.

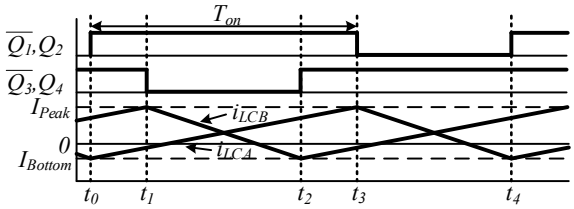

Fig. 2. Switching waveforms with the TCM operation.

$$P_{in} = \frac{V_{in}^{\ 2}}{L_C}\frac{D}{f_S} + 2V_{in}I_{Bottom} \quad \text{..... (1)},$$

where I_{Bottom} is the boost inductor bottom current, V_{in} is the input voltage, V_C is the boost capacitor voltage, L_C is the boost inductor, f_S is the switching frequency, P_{in} is the input power, and D is the duty ratio of the lower arm power devices on the primary H-bridge, and D is defined as

$$D = 1 - \frac{V_{in}}{V_C} \quad \text{..... (2)}.$$

Namely, the input power is expressed as

$$P_{in} = \frac{V_{in}^{\ 2}}{L_C}\frac{\left(1 - \frac{V_{in}}{V_C}\right)}{f_S} + 2V_{in}I_{Bottom} \quad \text{..... (3)},$$

where N is the turn ratio of the transformer, these are not flexibility parameters because V_{in} is decided by connected equipment, V_C must match the turn ratio of the transformer, L_C is designed to transmit the rated power with the TCM operation, and I_{Bottom} is decided by the negative current to achieve ZVS. Therefore, the switching frequency has to vary to change the input power. However, the switching frequency is limited by power device performance.

According to (3), input power is reduced by reducing V_C, keeping the switching frequency.

B. Full-Bridge Mode

Fig. 3(a) shows the steady-state waveforms of the Full Bridge (FB) mode of the proposed circuit. According to Fig.4, the FB operation has eight modes for a switching cycle.

In addition, only the half-switching cycle (mode I to IV)

of the analysis is enough because the transformer current is symmetrical. Therefore, the transformer current is expressed from (4) to (7) as

- Mode I ($0 \le \theta \le \delta$)

$$i_{Tr\_I}(\theta) = \frac{V_C}{\omega L_{DAB}}\theta - i_{Tr\_IV}(\pi) \quad \text{..... (4).}$$

- Mode II ($\delta \le \theta \le (1-2D)\pi$)

$$i_{Tr\_II}(\theta) = \frac{V_C - NV_{out}}{\omega L_{DAB}}(\theta - \delta) + i_{Tr\_I}(\delta) = 0 \quad \text{..... (5).}$$

- Mode III ($(1-2D)\pi \le \theta \le (1-2D)\pi + \delta$)

$$i_{Tr\_III}(\theta) = \frac{V_C}{\omega L_{DAB}}\left(\theta - (1-2D)\pi\right) + i_{Tr\_II}\left((1-2D)\pi\right)$$
$$\text{..... (6).}$$

- Mode IV ($(1-2D)\pi + \delta \le \theta \le \pi$)

$$i_{Tr\_IV}(\theta) = \frac{V_C - NV_{out}}{\omega L_{DAB}}\left\{\pi - \left((1-2D)\pi + \delta\right)\right\} + i_{Tr\_III}\left((1-2D)\pi + \delta\right) \quad \text{..... (7).}$$

where V_{out} is the output voltage, ω is the angular frequency, and δ is the phase shift angle between the primary side voltage and the secondary side voltage. The transmission power is expressed as

$$P_{Tr\_FB} = \frac{1}{2\pi}\int_0^{2\pi} v_{Pri}(\theta) i_{Tr}(\theta) d\theta = \frac{V_C^{\,2}}{\pi\omega L_{DAB}}\left(-\frac{1}{2}\delta^2 + 2\pi D\delta\right) \quad \text{..... (8),}$$

where v_{Pri} is the output voltage of the primary H-bridge. Note that (4) to (7) are valid when the switching duty D is 0.5 or less. When the switching duty exceeds 0.5, the formula becomes valid by replacing D with $(1-D)$.

C. Half-Bridge Mode

Fig. 3(b) shows the steady-state waveform of the Half Bridge (HB) mode of the proposed circuit. According to fig. 4, the HB operation has eight modes for a switching cycle. In the HB mode, only a half-switching cycle of the analysis is needed, as well as in the FB mode.

According to fig. 4, the HB mode applies a half voltage of the output voltage NV_{out} to the primary side of the transformer. Therefore, the transformer current is expressed from (9) to (12) as

- Mode I ($0 \le \theta \le \delta$)

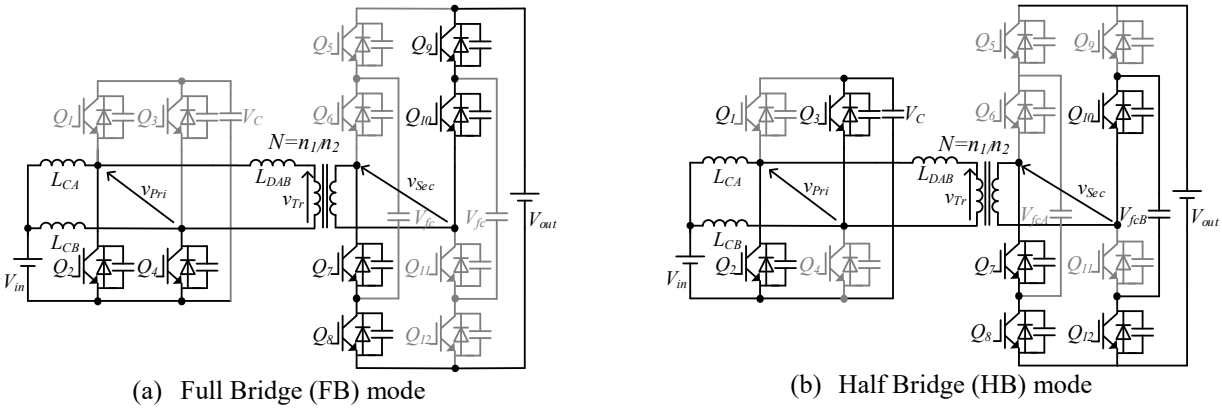

(a) Full Bridge (FB) mode (b) Half Bridge (HB) mode

Fig. 3. Switching Pattern of FB and HB mode.

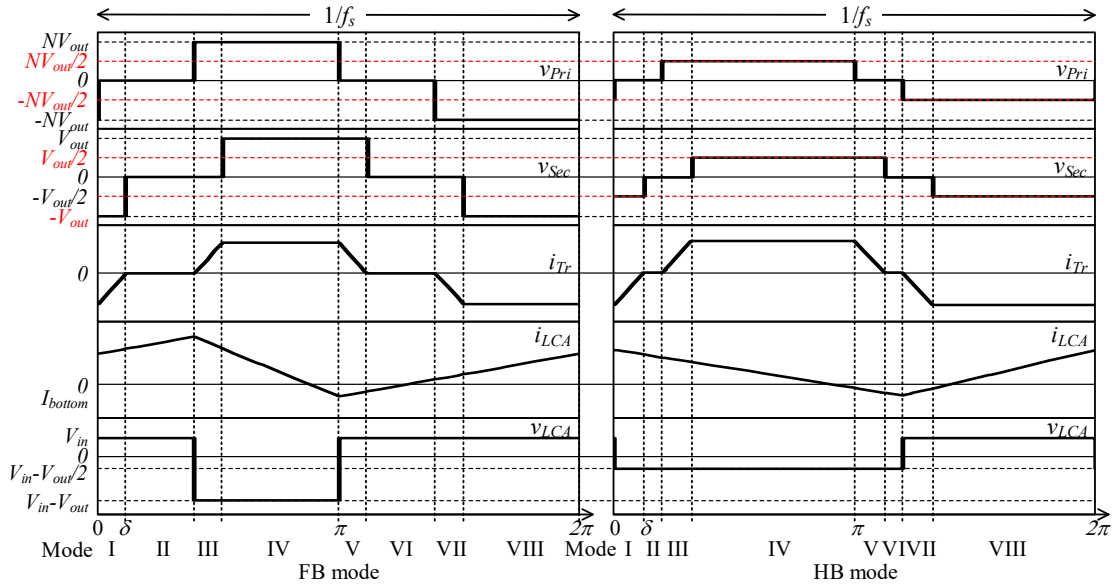

Fig. 4. Operation waveform of FB and HB modes

$$i_{Tr\_I}(\theta)=\frac{V_C}{\omega L_{DAB}}\theta-i_{Tr\_IV}(\pi) \quad \text{..... (9)},$$

- Mode II ($\delta \le \theta \le (1-2D)\pi$)

$$i_{Tr\_II}(\theta)=\frac{V_C-\frac{NV_{out}}{2}}{\omega L_{DAB}}(\theta-\delta)+i_{Tr\_I}(\delta) \quad \text{..... (10)},$$

- Mode III ($(1-2D)\pi \le \theta \le (1-2D)\pi+\delta$)

$$i_{Tr\_III}(\theta)=\frac{V_C}{\omega L_{DAB}}\left(\theta-(1-2D)\pi\right)+i_{Tr\_II}\left((1-2D)\pi\right) \quad \text{..... (11)},$$

- Mode IV ($(1-2D)\pi+\delta \le \theta \le \pi$)

$$i_{Tr\_IV}(\theta)=\frac{V_C-\frac{NV_{out}}{2}}{\omega L_{DAB}}\left\{\pi-\left((1-2D)\pi+\delta\right)\right\}+i_{Tr\_III}\left((1-2D)\pi+\delta\right) \quad \text{.... (12)},$$

Note that V_C is halved in voltage to match the voltage with $NV_{out}/2$. The transmission power is the same as in the FB mode, which is expressed as

$$P_{Tr\_HB}=\frac{1}{2\pi}\int_0^{2\pi} v_{\mathrm{Pr}i}(\theta)i_{Tr}(\theta)d\theta=\frac{{V_C}^2}{\pi\omega L_{DAB}}\left(-\frac{1}{2}\delta^2+2\pi D\delta\right) \quad \text{..... (13)},$$

The HB mode applies a half voltage of the output voltage V_{out} to the transformer. Therefore, the numerator in (13) becomes smaller; the input power is smaller under the same operating conditions as the FB mode. In other words, the TCM operation is achieved when the HB mode is applied in the low input power range, whereas the TCM operation is not achieved in the FB mode.

D. ZVS condition

Fig. 5 shows the operating waveform with the ZVS condition, which is determined by the difference between the boost inductor current and transformer current. In order to achieve ZVS, the following condition must be kept during the dead time period. The ZVS conditions are expressed as

$$I_{LCA}{}' < I_{Tr}{}' \quad \text{..... (14)},$$

$$\begin{cases} I_{LCA}{}' = I_{bottom}+\frac{V_{in}}{L_{CA}}T_d \\ I_{Tr}{}' = -\frac{V_C}{L_{DAB}}T_d \end{cases} \quad (D<0.5)$$

$$\begin{cases} I_{LCA}{}' = I_{bottom}+\frac{V_{in}}{L_{CA}}T_d \\ I_{Tr}{}' = \frac{V_C}{\omega L_{DAB}}\delta-\frac{V_C}{L_{DAB}}T_d \end{cases} \quad (0.5<D)$$

where $I_{LCA}{}'$ is the boost inductor current of A-leg at the end of dead time, L_{CA} is the boost inductor, and T_d is the dead time of the switching device.

According to Fig. 5(a), ZVS is achieved by the TCM operation under conditions where the switching duty D of the lower switch is less than 0.5. Because the lower limit of the transformer current is clamped to 0A by the zero-current period. However, in Fig. 5(b), the transformer current flows from zero current to negative current during the dead time period. Therefore, if the switching duty D of the lower switch is higher than 0.5, the boost inductor current must be smaller than the transformer current when the end of the dead time. Namely, under the non-ZVS conditions, the parasitic capacitance of the lower switch is recharged and hard switching.

E. TCM operating area in FB Mode and HB mode

The TCM operation is implemented using triangular modulation with the variable carrier frequency. The TCM operation requires the small negative inductor current to discharge the output capacitance of the IGBT during the dead time before being turned on. The boost inductor bottom current is expressed as

$$I_{Bottom}=\frac{C_{OES}V_C}{T_d} \quad \text{..... (14)},$$

where C_{OES} is the output capacitance of the IGBT, and T_d is the dead time. I_{Bottom} is designed to discharge enough from the parasitic capacitance. Also, the switching frequency is increased when the transmission power is decreased. Thus, the increase in the switching frequency is reduced by the duty ratio of the lower arm power device on the primary H-bridge being reduced. That is, the HB mode of the proposed method is applied to reduce the switching frequency at the light load conditions so that the TCM operation area is expanded.

Fig. 6 shows the TCM operation area of the FB and HB modes according to the input voltage and the input current

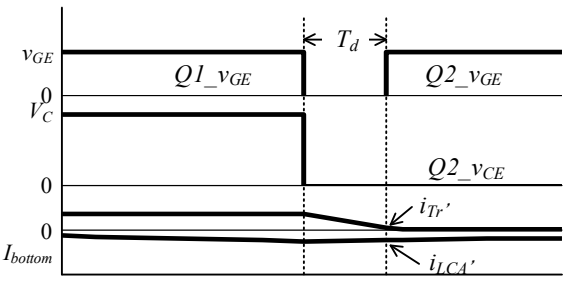

(a) ZVS operating waveform for $0.5 < D$ condition

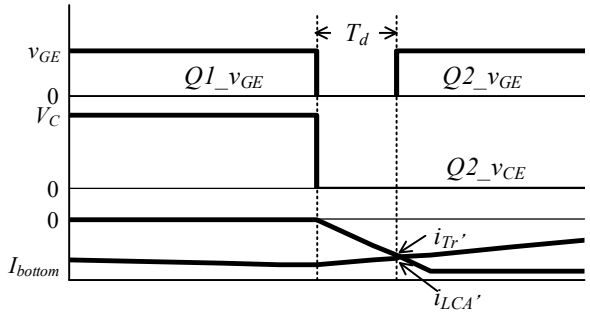

(b) ZVS operating waveform for $D < 0.5$ condition

Fig. 5. The relationship between transformer current and boost inductor current at each duty condition.

obtained by (3). In the FB mode, the TCM operation does not achieve in the light load condition due to the switching frequency limitation at 30 kHz. On the other hand, HB mode achieves the light load condition from 160 V to 320 V condition. In particular, the 320 V condition is maximum expanded by 70 % from 0.05 p.u. to 0.44 p.u. with the operation area. In addition, the ZVS operation is achieved in the light load region below 0.05 p.u. despite the CCM operation.

Fig. 7 shows the ZVS range of the FB and HB modes. According to Fig.7, ZVS is achieved in the FB mode over the full operating range. The hard switching occurs in the HB mode under conditions where the switching duty is less than 0.5. The ZVS range derives the boundary condition when I_{Tr}' and I_{LC}' are equal, which is expressed as

(when $D < 0.5$)

$$P_{in} = \frac{\left\{\begin{array}{l}\left(2L_{DAB}V_C{V_{in}}^2 + 2L_C{V_C}^2V_{in}\right)f_S T_d \\ +L_{DAB}{V_{in}}^3 - L_{DAB}V_C{V_{in}}^2\end{array}\right\}}{L_{DAB}L_C V_C f_S} \quad \text{..... (15),}$$

(when $0.5 < D$)

$$P_{in} = \frac{\begin{array}{l}2V_{in}\sqrt{\left(2L_{DAB}L_C{V_C}^2{V_{in}}^2 + 2L_C{V_C}^3V_{in}\right)f_S T_d} \\ +L_{DAB}L_C V_C{V_{in}}^3 - L_{DAB}L_C{V_C}^2{V_{in}}^2 \\ +\left(-2L_{DAB}V_C{V_{in}}^2 - 2L_C{V_C}^2V_{in}\right)f_S T_d\end{array}}{-L_{DAB}{V_{in}}^3 + L_{DAB}V_C{V_{in}}^2} \quad \text{.. (16).}$$

Therefore, the ZVS is achieved when the input power is smaller than (15) or (16). Note that the switching duty of more than 0.5 is ZVS in the full operating range because $i_{Tr} > i_L$ over the full operating area by applying the TCM.

IV. Efficiency Analysis

Table 1 shows the efficiency analysis and the experimental conditions. In this efficiency analysis, only power device losses are considered, i.e., the magnetic components losses, and so on, are not considered. The power device losses are calculated from the switching loss and the conduction loss, which is expressed as

$$\begin{aligned} P_{Loss} &= P_{con\_loss} + P_{sw\_loss} \\ &= V_{CE}I_C + E_S f_S \end{aligned} \quad \text{..... (17),}$$

where P_{Loss} is the power device losses, P_{con_loss} is the conduction loss, P_{sw_loss} is the switching loss, V_{CE} is the IGBT's collector-emitter saturation voltage, I_C is the collector current, and E_S is the switching energy. The collector-emitter saturation voltage is referenced from the datasheet. The switching loss becomes zero at the condition achieving an ideal ZVS operation because the energy of the output capacitance of IGBT is regenerated to the power supply or sent to the load. However, the other switching losses, not caused by the output capacitance, such as the loss caused by a tail current, remain. Therefore, the energy of the other loss can be obtained by

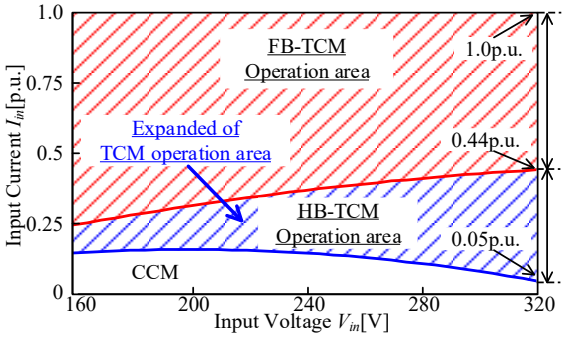

Fig. 6. The TCM operation area of FB mode and HB mode according to the input voltage and the input current

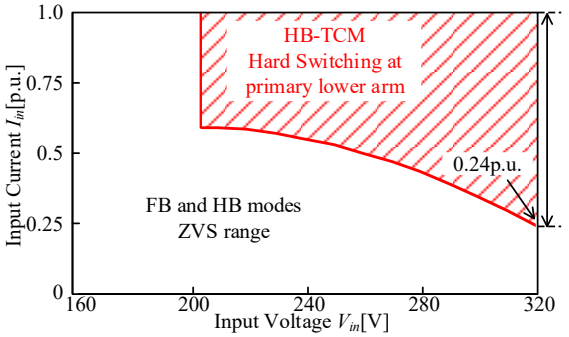

Fig. 7. The ZVS range of FB and HB modes

Table 1. The efficiency analysis and the experimental conditions.

Element	Symbol	Value
Rated power	P_{rated}	12.8kW @V_{in}=320V
Rated current	I_{rated}	40A
Switching frequency	f_s	(C-F DAB)10-30kHz (DAB) 10kHz
Input voltage	V_{in}	160-320V
Output voltage	V_{out}	1500V
Boost capacitor voltage	V_C	(HB mode) 400V (FB mode) 800V
Boost inductor	L_C	270μH
External inductor	L_{DAB}	45μH
Leakage Inductor	L_l	23.5μH
Magnetizing Inductance	L_{Mg}	48mH
Turn ratio	N	(C-F DAB) 0.532 (DAB) 0.26
Dead-time	T_d	1μs
Hybrid-SiC Modules		CMH150DY-24NFH

$$E_S = E_{off} - \frac{1}{2}C_{OES}V^2 \quad \text{..... (18),}$$

where E_{off} is the turn-off switching energy per pulse from the datasheet of the IGBT, and V is the collector-emitter voltage, which is 750V used in the calculation.

Fig. 8 shows the analyzed efficiency considering only power device losses. The switching losses dominate at

light loads due to the high ripple current in the boost inductor in the Current-Fed DAB converter with the TCM. Therefore, the light load efficiency is decreased in the FB mode, where the boost inductor current ripple is larger than that in the HB mode. According to Fig. 8(a), the analyzed efficiency considering only power device losses of the HB mode is 94 % at the output power of 0.1p.u.. The losses are reduced by approximately 21.8 % compared to that of the FB mode. In addition, the conventional method of the CCM improves the efficiency near the rating by using TCM because the ZVS is achieved at turn-on by using TCM. In the light load range, the use of the HB mode significantly improves efficiency because the HB mode reduces turn-off losses at light load by reducing the boost inductor current ripple.

Fig. 8(b) shows the breakdown of losses at the input voltage of 320 V and the output power of 0.1p.u.. The analysis results mention the primary side switching loss in the FB mode is 64 W. In contrast, the primary side switching loss in the HB mode is 41 W, which is approximately 35% less than that of the FB mode. In addition, the conduction loss is slightly increased by operating in the HB mode, but it is small enough compared to the decrease in the switching loss.

According to Fig. 8(c), in the FB mode, the efficiency analysis at rated current showed that 98% or higher efficiency was achieved in all voltage conditions and the maximum efficiency of 98.5 %. On the other hand, losses increase due to hard switching in the conventional modulation of the Current-Fed DAB. Although, the DAB converter had the maximum efficiency in Fig. 8(a). The efficiency drops significantly due to voltage fluctuations, especially in low-voltage conditions.

Fig. 8(a) clearly shows that the HB mode is unsuitable for the rated current operation. For this reason, Fig. 8(c) does not show the efficiency of the HB mode.

V. Experimental Results

In this section, the experimental results are demonstrated in order to evaluate the validity of the Current-Fed DAB Converter with a three-level flying capacitor converter. A 12.8-kW prototype (CMH150DY-24NFH, which is Si IGBT + SiC SBD used) is operated at the switching frequency of 10 kHz to 30 kHz, the input voltage of 160 V to 320 V and an output voltage of 1500 V.

Fig. 9 shows the operation waveform of the FB mode. According to Fig. 9(a), the output current of 1p.u., the input voltage of 320 V, the boost capacitor voltage of 800 V, and the output voltage of 1500 V. Note that the switching frequency is set to 15.5 kHz. The rated power operation is confirmed by the experiment. In Fig. 9(b) and (c), the output current is 0.75 p.u., and 0.5 p.u., respectively. Also, the phase shift angle between the primary side voltage and secondary side voltage is calculated. The phase shift angle of the theoretical value is 9.8 deg. while the experimental value is 8.1 deg. at the rated power. Meanwhile, the angle of the theoretical value is 8.7 deg. while the experimental value is 4.9 deg. at the 0.5 p.u. There are errors of 17% and 44% between the

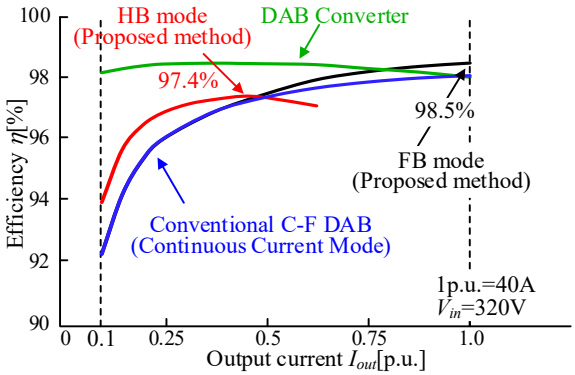

(a) Efficiency analysis of FB mode and HB mode at input voltage of 320 V.

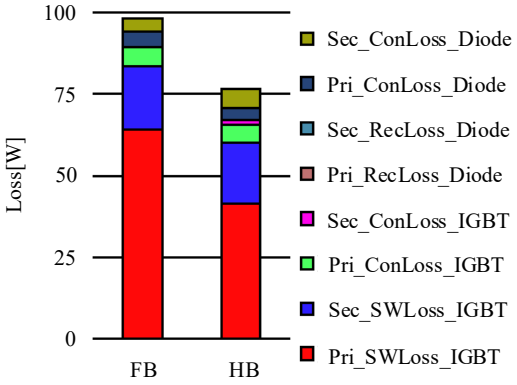

(b) Efficiency analysis of FB mode and HB mode at input voltage of 320 V and input current 0.1 p.u.

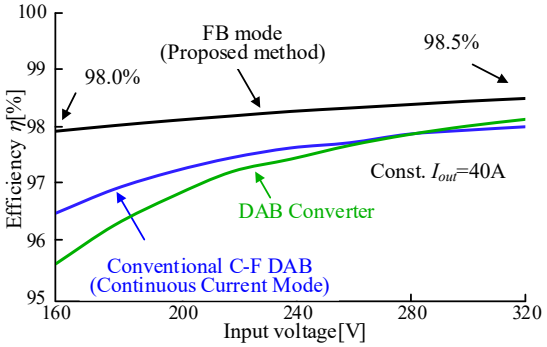

(c) Efficiency analysis of FB mode at rated output current conditions.

Fig. 8. Efficiency analysis of FB mode and HB mode at input voltage 320 V.

angle of the experimental waveform and the theoretical value, respectively. The cause of this phase shift angle error is the output capacitance of the IGBT and operating conditions error where the load current is small. The error compensation will be studied in the future.

Fig. 10 shows the operation waveform of the HB mode. According to Fig. 10(a), the output current of 0.43 p.u., the input voltage of 320 V, the boost capacitor voltage of 400 V, and the output voltage of 1500 V. Note that the switching frequency is set to 10 kHz. In Fig. 10(b), the output current of 0.3 p.u. and in Fig. 10(c), the output current of 0.2 p.u.. In the FB mode, the switching frequency of 30kHz is required to obtain the input power of 0.43 p.u.. The switching frequency required in the HB

mode is lower than that in the FB mode at light loads. The switching frequency is reduced by 66% at 0.43p.u. using the HB mode. According to Fig. 9 and Fig. 10, the negative current is kept constant by variable frequency control depending on the load, that is achieved the TCM operation.

Fig. 11 shows the efficiency characteristics with each operation mode at V_{in} = 320 V and V_{out} = 1500 V. The maximum efficiency of the experimental results for the FB and HB mode is 3.7% lower than the efficiency analysis because other losses except the power device are not considered, such as the transformer, and the inductor losses. The transformer current is increasing in the HB mode compared to the FB mode by the boost voltage of V_C is half. Therefore, the efficiency of the HB mode is higher than the FB mode at the light load where turn-off loss dominates the whole loss. In contrast, the efficiency of the FB mode is higher than the HB mode from the medium to rated loads where conduction loss dominates the whole loss. Fig. 11, the maximum efficiency of 94.8 % in the FB mode is achieved at the rated power. Also, the maximum efficiency of the HB mode is 93.7 % at the 43 % input current. Furthermore, the HB mode has a voltage polarity inversion during the dead time period. The polarity inversion occurs when the transformer current is equal to the boost inductor current. Also, the primary lower switch is hard-switching because of the voltage polarity inversion. More negative current of boost inductor is needed to achieve the ZVS, but the optimal inductor current should be considered in the future due to increased conduction loss.

VI. Conclusions

This paper proposed a three-level Flying Capacitor Current-Fed DAB converter for high output voltage applications(1500VDC). The proposed converter achieved

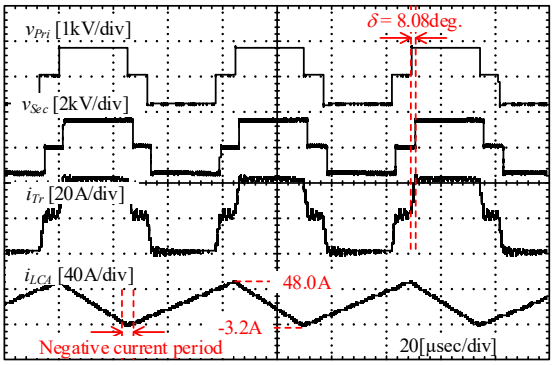

(a) V_{in} = 320V, I_{in} = 1.0p.u., f_S = 15.5kHz

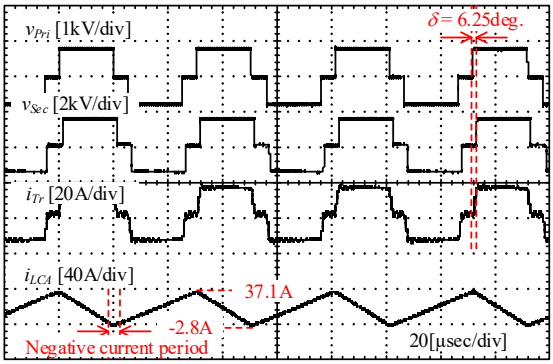

(b) V_{in} = 320V, I_{in} = 0.75p.u., f_S = 19.8kHz

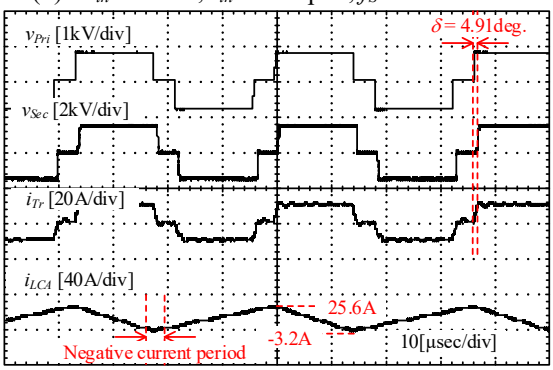

(c) V_{in} = 320 V, I_{in} = 0.5 p.u., f_S = 27.4kHz

Fig. 9 FB mode operation waveform of each input current conditions.

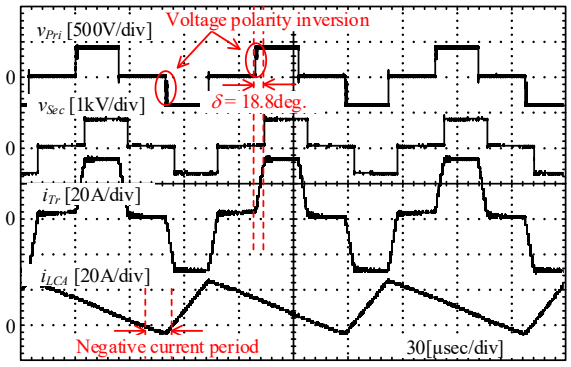

(a) V_{in} = 320V, I_{in} = 0.43p.u., f_S = 10.0kHz

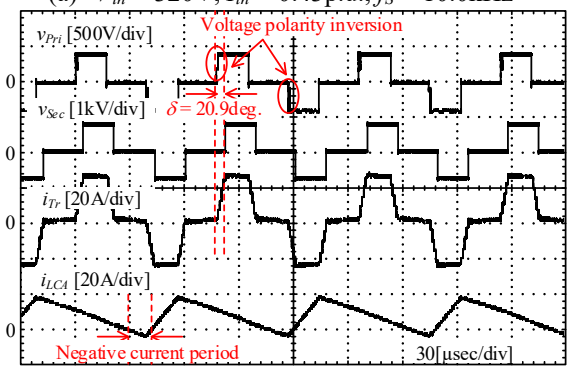

(b) V_{in} = 320V, I_{in} = 0.3p.u., f_S = 12.8kHz

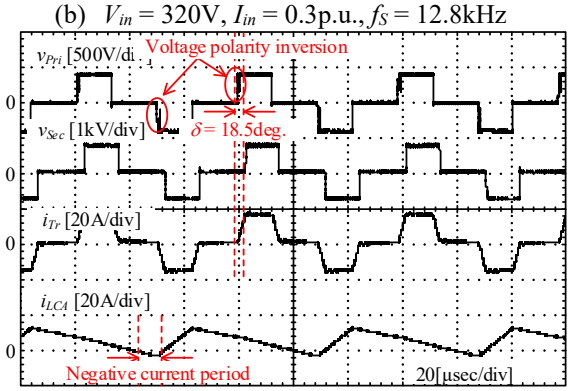

(c) V_{in} = 320 V, I_{in} = 0.2 p.u., f_S = 16.9kHz

Fig. 10 HB mode operation waveform of each input current conditions.

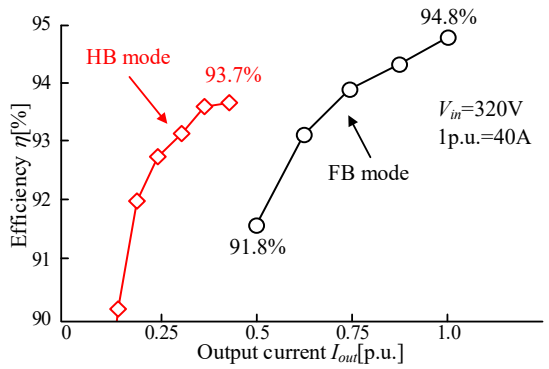

Fig. 11. Efficiency characteristic of FB mode and HB mode at input voltage of 320 V.

the TCM operation area over the wide transmission power range by the FB mode and the HB mode. In particular, it was confirmed that with the application of the HB mode, the TCM operation area was extended to 70 %. The validity of the proposed method was demonstrated by a 12.8-kW prototype circuit with Silicon IGBTs.

The maximum efficiency was 94.8 % of the FB mode at rated power conditions. On the other hand, the maximum efficiency was 93.7 % of the HB mode at the input voltage of 320V and the input current of 0.44 p.u. From the experiment, the TCM was achieved with a constant negative current by the variable switching frequency control. The light load efficiency was also improved by the HB mode compared to the FB mode from the efficiency analysis result and the experiment. The future works are the following, to obtain efficiency characteristics at other voltages and, load conditions; loss separation including iron loss; the compensation method for transmission power error, caused by the IGBT's output capacitance.

REFERENCES

[1] S. Sathyan, H.M. Suryawanshi, A.B. Shitole, M.S. Ballal, and V.B. Borghate, "Soft-switched Interleaved DC-DC Converter as Front-End of Multi-Inverter Structure for Micro Grid Applications", *IEEE Trans. on Power Electronics,* Vol. 9, No. 9, pp. 7645-7655, September 2018.

[2] K. kanathipan, and J. Lam, "A High Voltage Gain Isolated PC Micro-Converter With a Single-Voltage Maximum Power Point Tracking Controll Loop for DC Micro-Grid Systems", *IEEE Journal of Emerging and Selected Topic in Industrial Electronics*, Vol. 3, No. pp. 755-765, July 2022.

[3] Y. Tanahashi, H. Kobayashi, Y. Nakamura, and M. Aoki, "Practicality Assessment of MILP and PSO and Evaluation of Hybridized Method in Operational Plans for Microgrid System", *IEEJ Trans. on Industry Applications,* Vol. 142, No.12, pp. 897-906, 2022.

[4] M.T. Daniel, S. Krishnamoorthy, and N.E. Enjeti, "A New Wind Turbine Interface to MVdc Collection Grid With High-Frequency Isolation and Input Current Shaping", *IEEE Journal of emerging and selected topics in power electronics*, vol. 3, Issue 4, June 2015.

[5] T. Ishibashi, T. Jimichi, A. Iwata, and Y. sato, "High-Voltage DC/DC Converter with Twi-Series, Three-Parallel Connected IGBTs", *IEEJ Trans. on Industry Applications,* Vol. 139, No.6, pp. 597-605, 2019.

[6] M.M. Haque, P. Wolfs, S. Alahakoon, B.C.P. Sturmberg, Mithulananthan Nadrajah, and F. Zare, "DAB Converter With Q Capability for BESS/EV Applications to Allow V2H/V2G Services", *IEEE Trans. on Industry Applications,* Vol. 58, No. 1, pp. 468-480 January/February 2022.

[7] S. Chaurasiya, and, B. Singh, "A Bidirectional Fast EV Charger for Wide Voltage Range Using Three-Level DAB Based on Current and Voltage Stress Optimization", *IEEE Trans. on Transportation Electrification*, Vol. 9, No. 1, pp. 1330-1340, March 2023

[8] Y. Liu, K. Chen, N. Dung, C. Chen, Y. Syu, and P. Huang "Six-Switch Bridge CLLC Bidirectional Converter for Energy Storage Systems", *IEEJ Journal of Industry Applications*, Vol. 10, No.2, pp. 202-213, 2021.

[9] P. Liu, and S. Duan, "A ZVS Range Enhancement Strategy for the DAB Converter by Using Blocking Capacitors", *IEEE Journal of Emerging And Selected Topics In Power Electronics*, Vol. 9, No. 2, pp. 1389-1398, Aprirl 2021.

[10] G. Xu, L. Li, X. Chen, Y. Liu, Y. Sun, and M. Su, "Optimized EPS Control to Achieve Full Load Range ZVS With Seamless Transition for Dual Active Bridge Converters", *IEEE Trans. on Industrial Electronics*, Vol. 68, No. 9, September 2021.

[11] L. Gong, X. Jin, J. Xu, Z. Deng, H. Li, T.B. Soeiro, and Y. Wang, "A Dynamic ZVS-Guaranteed and Seamless-Mode-Transition Modulation Scheme for the DAB Converter That Maximizes the ZVS Range and Lowers the Inductor RMS Current", *IEEE Trans. on Power Electronics*, Vol. 37, No. 11, pp. 13119-13134, November 2022.

[12] F. Krismer, and J.W. Kolar, "Closed Form Solution for Minimum Conduction Loss Modulation of DAB Converters", *IEEE. Trans. on Power Electronics,* Vol. 27, No. 1, pp. 174-188, January 2012.

[13] O. Kwon, K. Kim, and B. Kwon, "Highly Efficient Single-Stage DAB Microinverter Using a Novel Modulation Strategy to Minimize Reactive Power", *IEEE Journal of Emerging and Selected Topics in Power Electronics,* Vol. 10, No. 1, pp. 544-552, February 2022.

[14] R. Kondo, Y. Higaki and, M. Yamada, "Experimental Verification of Reducing Power Loss under Light Load Condition of a Bi-Directional Isolated DC/DC Converter for a Battery Charger-Discharger of Electric Vehicle", *IEEJ Journal of Industry Applications*, Vol.10, No.3 pp. 377-383, 2021.

[15] H. Higa, S. Takuma, K. Kusaka, and J. Itoh, "Development of T-type Dual Active Bridge DC-DC Converter" *IEEJ Trans. on Industry Applications*, Vol. 139, No. 4, pp. 388-400, 2019.

[16] Y. Tashiro, and, H, Haga, "Improvement of Light-Load Efficiency by using a Six-Arm Converter with Series-Parallel Switching", *IEEJ. Journal of Industry Applications,* Vol. 10, No. 2, pp. 273-281, 2021.

[17] Y. Xuan, X. Yang, W. Chen, T. Liu, and X. Hao, "A Three-Level Dual-Active-Bridge Converter With Blocking Capacitor for Bidirectional Electric Vehicle Charger", *IEEE. Access*, Vol. 7, December 2019.

[18] D. Sha, G. Xu, and Y. Xu, "Utility Direct Interfaced Charger/Discharger Employing Unified Voltage Balance Control for Cascaded H-Bridge Units and Decentralized Control for CF-DAB Modules" *IEEE Trans. on Industrial Electronics,* Vol. 64, No. 10, pp. 7831-7841, October 2017.

[19] Y. Shi, R. Li, Y. Xue, and H. Li, "Optimized Operation of Current-Fed Dual Active Bridge DC-DC Converter for PV Applications", *IEEE. Trans. on Industrial Electronics,* Vol. 62, No. 11, pp. 6986-6995, November 2015.

[20] H. Watanabe, A. Tamagawa, and J. Itoh, "Efficiency Improvement of Current-Fed DAB converter by Triangular Current Mode for Wide Voltage Application", *The 2022 International Power Electronics Conference (IPEC-Himeji 2022- ECCE Asia)*, July 2022.